Exploring the performance of experimentally benchmarked RC bridge pier models when subjected to sequential seismic shocks

Xiao Ge[1,2*], Mohammad M. Kashani[3], Zhi-Guo Sun[4], Yu-Qing Yang[5], Nicholas A. Alexander[6]

Abstract

In this paper we explore the performance of RC bridge piers to seismic ground motion sequences, using both experimental and numerical models. Four RC columns were tested on the University of Bristol's shake table. These columns contained both well-confined and poor-confined cases. Spectrally matched by near-field without pulse (NFWP), near-field pulse-like (NFPL) and far-field (FF) ground motion records where employed in a sequential/progressive fashion ranging from (I) slight damage (II) extensive damage (III) complete damage and (IV) aftershock cases. These experimental test results are then used to develop a benchmarked *OpenSees* model of this bridge pier. The importance of the concrete tension constitutive model is highlighted. The differences between sequential (progressive damage) and neglecting sequential seismic events are discussed. The benchmarked model is then used for a heuristic case using incremental dynamic analyses. A comparison is made between drift and energy dissipation performance measures, that suggests drift cannot identify the increased system damage induced by sequential events.

Keywords: RC bridge piers, mainshock-aftershock sequences, finite element modelling, drift,

[1] School of Civil and Transportation Engineering, Hebei University of Technology, Tianjin, 300401, China

[2] Earthquake Engineering Research and Test Center, Guangzhou University, Guangzhou, 510006, China

[3] Faculty of Engineering and Physical Sciences, University of Southampton, Southampton, SO17 1BJ, United Kingdom

[4] Key Laboratory of Building Collapse Mechanism and Disaster Prevention, China Earthquake Administration, Sanhe, 065201, China

[5] School of Civil and Resource Engineering, University of Science and Technology Beijing, Beijing, 100083, China

[6] Department of Civil Engineering, University of Bristol, Bristol, BS8 1TR, United Kingdom

* Coresponding author: Xiao Ge (xiao.ge@aol.co.uk)

energy dissipation, shaking table test

1. Introduction

Sequential seismic events have caused tremendous economic losses and life safety threat in recent years (the 2008 Wenchuan earthquake; the 2011 Tohoku earthquake; the 2016 central Italy earthquake). Concerns about seismic behaviour of structures under the excitation mainshock-aftershock (MSAS) have been raised [1,2]. In performance-based seismic design, drift ratio is the most commonly used engineering demand parameter (EDP) to predict the seismic performance of structures. However, in the case of catastrophic earthquake mainshock-aftershock sequences, does the drift ratio adequately reflect the structural damage? The non-linear dynamic responses of structures excited by mainshock-aftershock (MSAS) earthquakes have been investigated by many researchers. The peak ductile demand of structures excited by sequential earthquakes is investigated [1]. It has been found that the peak displacement of structures excited by real sequential earthquakes is about 5%-20% higher than that excited by mainshock only [1]. Some researchers [3,4] found that structural responses are similar during aftershocks when the structure is subjected to ground motion records with the same aftershock but different mainshocks. Irregular structures exhibit more sensitivity than regular structures in MSAS sequences direction [5]. Irregular structures show high drift demands than regular structures in aftershocks in some cases [5]. Aftershock polarity/direction effects on structural responses are investigated by some researchers [4–6]. Due to the residual displacement and damage caused in mainshock, different polarities can result in different drift demands. Some works [7–9] indicate that the relative PGA of aftershock to mainshock does not have a significant influence on the structural degradation.

In performance-based seismic design, a precise structural model is crucial. Many investigations have been done to explore the adaption of numerical models of RC bridge piers [2,10,19,11–

18]. Lumped-plasticity element, distributed inelasticity element with force-based formulation and distributed inelasticity element with displacement-based formulation are most commonly used modelling strategies. Rodrigues et al. [11] suggest that lumped-plasticity modelling strategy has easier discretisation and lower computational cost. However, Kashani et al. [10] found distributed inelasticity modelling strategy is more generic. He et al. [12] reviewed the optimal size of force-based element of concrete component and found with optimal element size, the non-objective curvature prediction can be avoided. To get better modelling of structural strength degradation, the effects of buckling and fatigue on reinforcement are taken into account in the modelling process by some researchers. However, the buckling model relies on precise calibration, which is not always available in practice [11]. To simulate long-service structures, corrosion effects are considered by many researchers. In some cases, the structures are subjected biaxial excitation, torsional movement could occur. Therefore, multiple excitation effects are explored by some researchers. With all the development of structural modelling, predicting the nonlinear behaviour of RC structures is still challenging. The blind prediction contest held by Pacific Earthquake Engineering Research Centre (PEER) shows scatter results in terms of peak drift, shear force and energy dissipation with different modelling strategies, although the excitation and target structure are exactly same [20].

In this paper, a numerical finite element model based on the Open System for Earthquake Engineering Simulation (*OpenSees* [21]) is introduced. The model is assembled by several force-based inelastic elements. The length of the element with the plastic hinge is determined based on the recommendation of Kashani et al [10,22]. A rigid element is applied to simulate the superstructures of the bridge pier. To model the strain penetration effects, a zero-length element is applied. A tensile branch of concrete strain-stress model is added to the confined concrete core model to account for the tensile behaviour of the concrete core during earthquake events. The proposed model is benchmarked by the shaking table tests conducted by the authors previously [23]. With this updated *OpenSees* model, a set of incremental dynamic analyses (IDA) is carried out for multiple mainshock-aftershock (MSAS) sequences with different ground motion types and different mainshock to aftershock peak ground motion acceleration (PGA) ratios. The differences in peak drift and dissipated energy, as performance damage measures in IDA is evaluated.

Thus, this paper explores the utility of using drift as a proxy for damage in the case of (i) this class of system (ii) the best available, experimentally benchmarked numerical models and (iii) mainshock-aftershock sequences that produce progressive deterioration of the system.

2. Numerical model of RC bridge piers

2.1 Experimental configuration of RC bridge piers

In the authors' previous study [23], to investigate the influence of ground motion characteristics and structural detailing, two types of rectangular RC columns are designed for a set of large scale shaking table tests (see Fig. 1). The one is well confined with a transverse tie spacing of 80 mm based on the requirement of modern seismic design code (i.e. Eurocode2 [24], Eurocode8 [25]). The other one with lighter confinement (200 mm spacing) is designed to represent old RC bridge piers. Both types of the column have a cross-section of 250 × 250 mm. The height is designed as 2300 mm. The column is cast on a foundation of 700 mm in height, 300 mm in depth and 1500 mm in width. The compressive test on the concrete cylinder specimen indicates the average uniaxial strength is 30 MPa. The properties of the reinforcing steels are listed in Table 1.

Table 1. The mechanical properties of reinforcing steel bars.

Bar diameter	8 mm	16 mm
Yield strain	0.00261	0.002733
Yield stress (MPa)	520	530
Elastic modulus (MPa)	200426	193913
Hardening strain	N/A	0.02547
Strain at maximum stress	0.05660	0.164800
Maximum stress (MPa)	645	640
Fracture strain	0.151800	0.227350

Fig. 1. The setup of the shaking table test.

2.2 Discretisation of the *OpenSees* model

A numerical finite element (FE) model based on *OpenSees* is proposed to simulate the seismic behaviour of rectangular RC bridge piers. It is based on fibre model due to the high accuracy compared with lumped model and distributed non-linearity model. The discretisation of the rectangular RC column model can be found in Fig 2. The model is assembled by four elements: (i) the zero-length section element representing the connection between the RC column and the footing; (ii) the element I where the plastic hinge happens; (iii) the element II of that the response is almost linear; and (iv) the rigid element representing the metal mass blocks applied on column top. The detailed descriptions of the elements, the sections, the materials and the boundary conditions can be found in following parts.

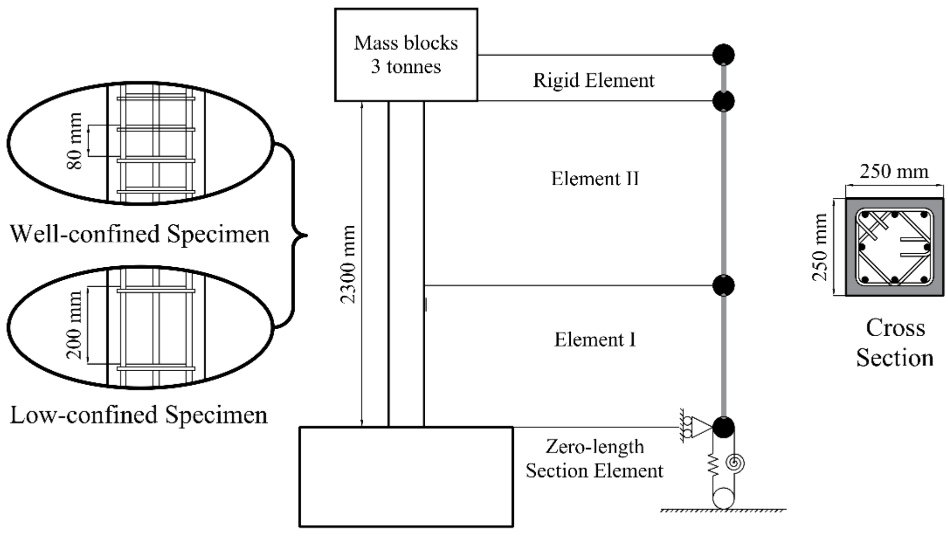

Fig. 2. The schematic of the specimen and the discretisation of the proposed model.

2.3 Displacement-based vs force-based elements?

The non-linear analysis of the finite element model is based on either displacement or force formulations. The classical integration relies on the displacement-based formulation due to its easiness of implementation. This formulation estimates the nodal displacement along the objective structure. Some researchers [26] suggest to use multiple elements to guarantee accuracy due to displacement-based formulation cannot deal with a member with high nonlinearity. However, a member with multiple displacement-based elements could lead to the inaccuracy of plastic hinge estimate due to the error of the nodal displacement cumulation, which significantly reduces the reliability of the modelling result [26]. The increasing elements could also result in higher computational cost. Due to the highly non-linear nature of the structural behaviour in seismic events, force-based elements are utilised in this work. Force-based formulations allow the spread of the non-linearity along with the member. It relies on stress approximation along with the element. The accuracy of force-based formulations can be improved by increasing either element quantity or the integration points within each element. It is worth mentioning that increasing the number of integration points can reduce the numerical stability (i.e. resulting in convergence problems) of the computational model.

2.4 Viscous damping model

In the non-linear dynamic analysis of structures, the Rayleigh model is the most commonly used one to simulate damping behaviour. It contains a mass-proportional part and stiffness-proportional part (see Eqn. 1).

$$C = \alpha_M M + \alpha_K K \tag{1}$$

The coefficients α_M and α_K can be used to calculate the damping ratio ξ along with the natural frequency of the structure ω (Eqn. 2).

$$\xi = \frac{\alpha_M}{2\omega} + \frac{\alpha_K \omega}{2} \tag{2}$$

The accuracy and reliability of Rayleigh damping model is always a concern of researchers and engineers [27–33]. In response history analysis (RHA) of structure, the model cannot precisely reflect the damping behaviour due to its imperfect performance in inelastic response modelling. Charney [28] summarised three approaches of determining the stiffness term of Rayleigh damping model: (*i*) initial stiffness matrix, (*ii*) tangent stiffness matrix, and (*iii*) last-committed stiffness matrix. The *OpenSees* provides a sparse pattern for the damping matrix based on all the three methods mentioned above. Many researchers [27–33] encounter spurious structural response when they use initial stiffness matrix to compute damping of a structure subjected to earthquake excitation. The initial stiffness matrix [method (*i*)] cannot precisely determine the peak and displacement and plastic hinge rotation. It is also reported that in a softening element, which is the case in this work, initial linear stiffness can lead to large damping forces compared to restoring forces [27]. Tangent and Last-committed stiffness matrix (methods *ii* & *iii*) are reported as a reliable method in some cases. Both methods rely on tangent stiffness matrix. The key difference between methods (*ii*) and (*iii*) is that the coefficients of the stiffness-proportional in method *iii* is recomputed when the stiffness changes, while in method *ii*, the two coefficients are constant. In this work, Last-committed stiffness matrix (method *iii*) is selected. Hall [27] points out that with the mass-proportional term in the damping model, extraneous damping forces may be produced by the numerical model, especially in the cases when the target structure has superstructures. Therefore, according to Hall's recommendation [27], the coefficient of mass-proportional term (α_M) is set to 0 in this work. With Eqn. 2, the initial coefficient of stiffness-proportion term (α_K) can be obtained. It worth mentioning that Chopra and McKenna [30] pointed out that in case of large plastic deformations the sensitivity of the damping model is very limited, but some small viscous damping is helpful to provide numerical stability for the case of small pseudo-linearly elastic responses.

2.5 Uniaxial materials models

The material model of *Conrete02* in the *OpenSees* is employed in the proposed finite element model for the concrete cover. This material model is based on modified Kent and Park's model [34]. The concrete strength and corresponding strain are obtained by compressive tests of the concrete cylinder specimens. The elastic module (E_c) is determined by Eqn. 3.

$$E_c = 4700\sqrt{f_c} \tag{3}$$

where f_c is the compressive strength of concrete (unit: MPa). The ultimate strength of the concrete is designated as 20% of the concrete strength. The modified Kent and Park model account for the effect of tensile behaviour of the concrete. The model assumes the post-peak curve in tension branch is linear. The tensile strength (f_t) and the tension softening elastic module (E_{ts}) are defined in Eqns. 4 & 5.

$$f_t = 0.34\sqrt{f_c} \tag{4}$$

$$E_{ts} = \frac{f_t}{0.002} \tag{5}$$

The concrete core and cover are defined separately. The materials model of *Confinedconcrete01* is used in the proposed model to represent the concrete core with confinement. The model is based on Braga-Gigliotti-Laterza model (i.e. BGL model) [35,36]. Compared with the previous confined concrete models, the BGL model considers the bending stiffness of the vertical reinforcement. The classic models only consider the vertical bar effects on the effectiveness of confinement. The classic models only evaluate the effects of the transverse hoops by their volume against the confined concrete volume. However, the BGL model highlights the importance of considering the confinement diameter and hoop spacing variety caused by different deployment strategies of transverse hoops. With these improvements, the BGL model is believed have better performance of compressive confined concrete behaviour modelling. The main drawback is that the BGL model does not consider the tensile behaviour of confined concrete. Braga et al. [35] believe the tensile behaviour of concrete model does not have significant influence on the global behaviour of RC structures. However, given the strain-stress curves of concrete, this assumption only works for RC structures with large strain response. If the strain response is small (i.e. linear response), the tensile behaviour plays an important role. Neglecting the tensile behaviour can underrate the stiffness of the RC structures.

To solve the problem provoked in finite element analysis of RC structures with small linear response, a tensile branch of concrete strain-stress curve of the *Conrete02* model is added to the *Confinedconcrete01* model as a parallel material model. Essentially, the modified *ConfinedConcrete01* is a combination of the *ConfinedConcret01* and the tensile branch of the *Concrete02*. To estimate the tensile properties of confined concrete, an amplifying factor is applied to the tensile strain-stress curve of the unconfined concrete. It should be noted that the material model with only tensile behaviour is not provided in the *OpenSees*. Therefore, the compressive branch of the *Concrete02* model will be added as well. To avoid the impact of this unexpected compressive branch of the strain-stress curve. A down-scale factor of 1e-20 is applied. The strain-stress relation of the combined concrete model is shown in Fig. 3.

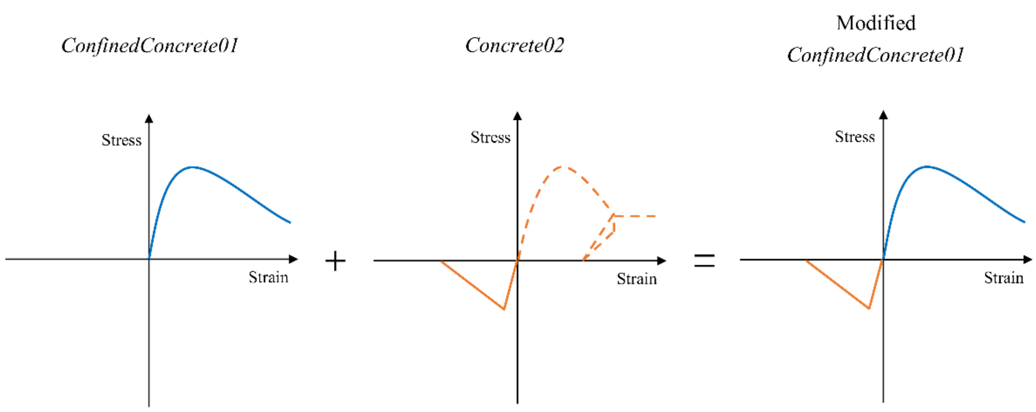

Fig. 3. The strain-stress constitutive relationship of concrete core (compression positive)

Giuffré-Menegotto-Pinto model [37] is adopted in the proposed model for reinforcement. It is known as *SteelMPF* [38] in the *OpenSees*. The key feature of this model is the assumption of isotropic strain hardening after the steel bar yield. A strain-hardening ratio, defined as the ratio of post-yield and initial Young's modulus, is introduced. The ratio is set to 0.01 as recommended. The transition from the elastic stage to the plastic stage can be customised to indicate the non-linearity. This gives more accurate results than *Steel01*, which is defined as a bilinear strain-stress relation curve. The yield strength is obtained by monotonic tensile tests of the steel bar specimens. The effects of low-cycle fatigue on the steel bars are considered in this work. A modified rainflow cycle counting algorithm based on Miner's Rule is applied on *SteelMPF* to accumulate damage [39,40].

2.6 Strain penetration model of foundation connection

The RC column is designed to be fully anchored into the concrete footing. However, in practice, the rotation at the interface of the column end and the footing cannot be avoided. This rotation is believed caused by the strain penetration of the vertical reinforcement. Zhao and Sritharan [41] developed a numerical hysteresis model of strain penetration effect. It is known as *Bond_SP01* in *OpenSees*. The material model *Bond_SP01*, as a supplementary model to the concrete and steel material models, is assigned to the zero-length section element. To define the slip response with respect to vertical reinforcement stress, the rebar slip under yield stress (S_y/mm), the ultimate slip (S_u/mm), the initial hardening ratio (b) and a pinching factor (R) are needed. The rebar slip under yield stress (S_y) is given by Eqn. 6:

$$\mathrm{S}_y = 2.54\left(\frac{d_b}{8437}\frac{f_y}{\sqrt{f_c}}(2\alpha+1)\right)^{\frac{1}{\alpha}} + 0.34 \tag{6}$$

where α and d_b (unit: mm) denote the parameter used in the local bond-slip relation and the diameter of the longitudinal rebars. In Eqn. 6, f_y refers to the yield strength of rebars (unit:

MPa). In this work, α is set to 0.4 as recommended in Ref. [41].

3. Model benchmarking using shaking table test sequences

Traditional model calibration relies on cyclic load tests of corresponding specimens. However, the degradation of structures excited by cyclic load shows a gradual trend, while a real earthquake can result in abrupt degradation due to sudden acceleration variating in ground motion trace. Therefore, in seismic analysis, a traditionally calibrated model could lead to spurious simulation results. The authors conducted a set of shaking table tests on the specimens mentioned above. To examine the influence of non-stationary characteristics of different types of ground motions, three ground motion records, namely, Northridge, Imperial Valley and Manjil earthquakes, are selected from NGA-West2 database [42] to represent near-field without pulse (NFWP), near-field pulse-like (NFPL) and far-field (FF) ground motions, respectively. In order to explore the non-ergodic properties of different ground motion records, the three seed records are matched to a target spectrum through RVSA developed by Alexander et al. [43]. The matched ground motion traces are shown in Fig 4. Each specimen is tested under the ground motion with scale factors of 25%, 300% and 500%. These scale factors represent slight, extensive and complete damage levels, respectively. After complete damage level (500% PGA), another round of test is conducted with ground motion factor of 300%. This is to investigate the seismic behaviour of damaged RC bridge piers in aftershock events. Due to the fact that each round of the test is conducted separately, a decrement of the vibration should be considered after each test. Ideally, it will take infinite time for the vibration decreases to zero. We assume the column is static, when the vibration reaches to 1% of the last-state amplitude in the shaking table test. This process is estimated as about 4 s. Therefore, 4-second input signal with 0-

amplitude is added between each two conjunct tests to the input signal used in numerical modelling.

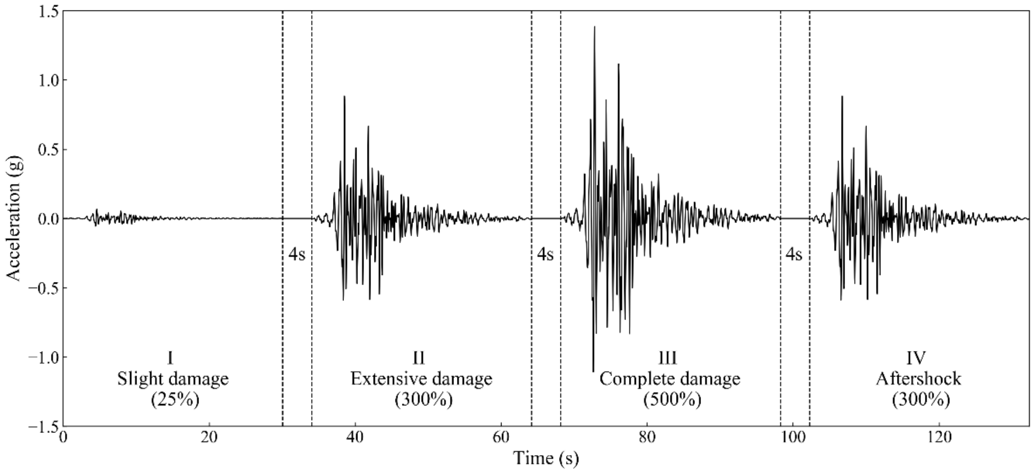

(a)

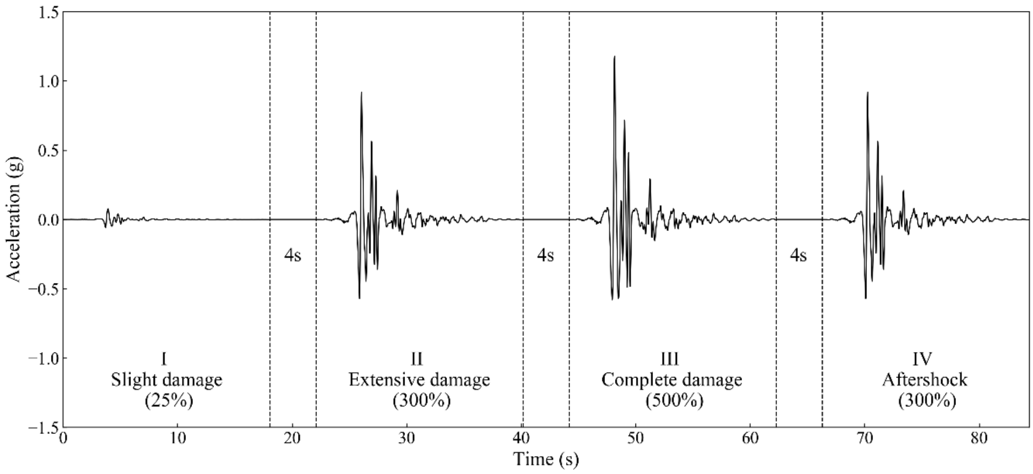

(b)

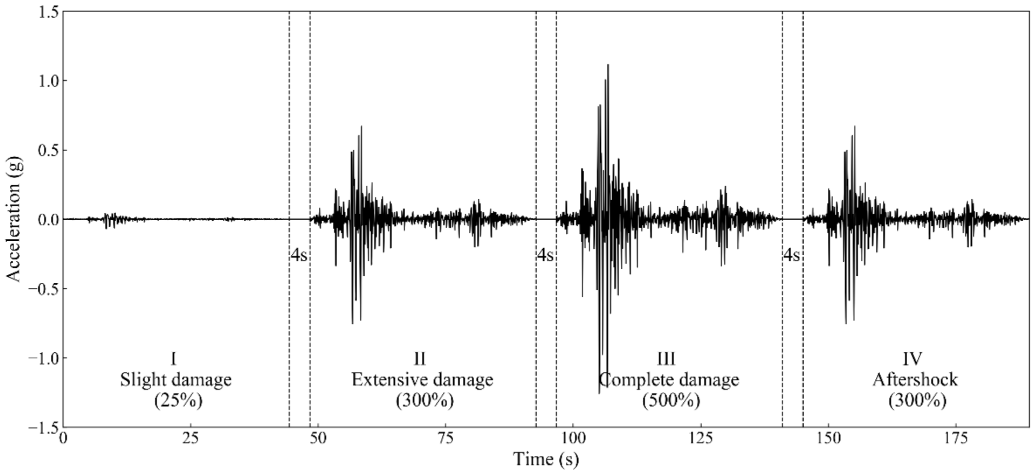

(c)

Fig. 4. The combined spectrally-matched input ground motion records of

(a) NFWP, (b) NFPL and (c) FF.

The results of the experimental work suggest the yielding of reinforcement steel does not have a significant impact on the global behaviour of RC columns. The insufficient confinement can lead to the premature concrete cover spalling and core crushing. It is also found that different types of ground motion (although with the same PGA) can result in different levels of peak deformation. The more detailed findings of the shaking table tests can be found in the authors' previous work [23].

With the recorded acceleration and displacement time-histories, the performance of the proposed FE model is calibrated. The displacement of the column is normalised to drift by the column height (2300 mm). The base shear is normalised by the axial load (3 tonnes).

In slight damage level (25%) test, with the *Confinedconcrete01* model alone in the concrete core, the numerical FE model significantly overestimates the seismic responses of the column in both displacement and acceleration manners. It illustrates the disadvantage of BGL model mentioned above. The improved concrete core material model can count for the tensile behaviour of the RC column before the core starts cracking. Therefore, the simulated results are in good agreement with the experimental results except the NFWP specimen. It should be mentioned that the NFWP specimen was slightly damaged in experimental preparation. The slight damage did not affect the follow-up shaking table tests. However, in slight damage level (25%) test, the slight damage has caused crack in concrete core. Therefore, the column has already lost the tensile capacity. The material model without considering tensile behaviour shows better modelling result in this exceptional case. The comparison of experimental results and modelling results with/without considering tensile behaviour can be found in Fig. 5.

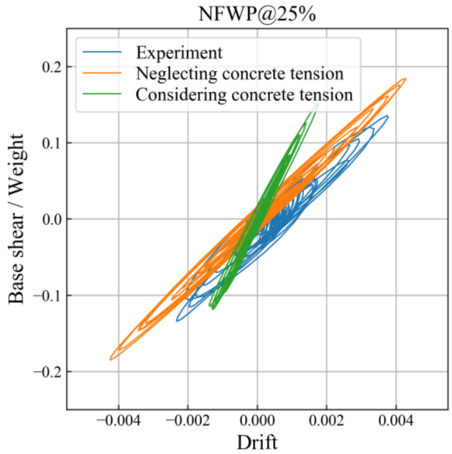

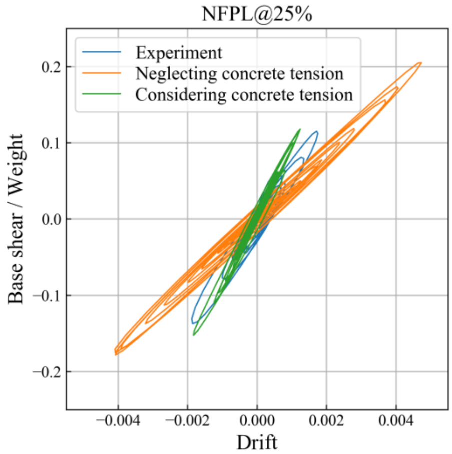

(a) (b)

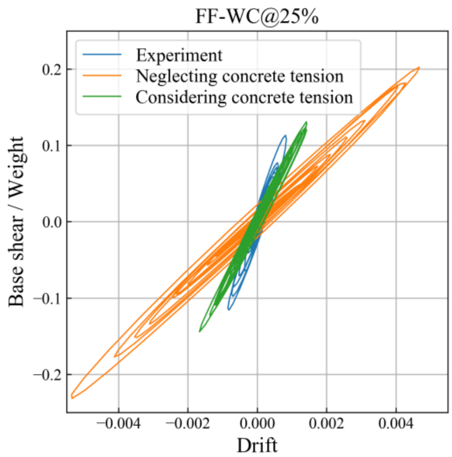

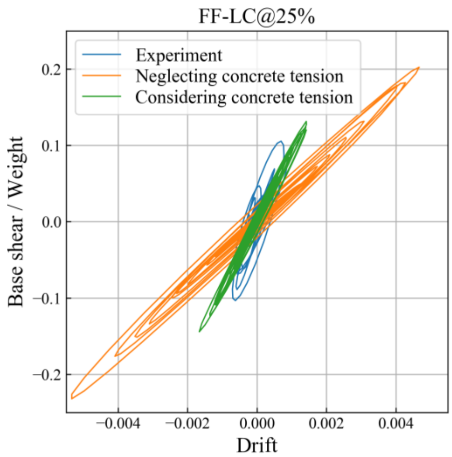

(c) (d)

Fig. 5. Numerical results with/without considering concrete tensile behaviour against the experimental results in slight damage level (25%).

In cases of extensive (300%) and complete (500%) damage levels, two modelling strategies are considered (i.e. direct modelling and modelling in MSAS sequence). The experimental and numerical time-histories of normalised force and displacment of the FF-LC column in 300% test is taken as an example (see Fig. 6). In extensive damage level tests, two modelling strategies show minors difference against the experimental results (see Fig. 7). This is because the slight damage level tests prior to the extensive damage level tests did not lead to much degradation of the specimens. The columns still have most of their seismic capacity. The result shows without considering the sequential effects, the proposed model can give a good simulation of RC columns that have experienced a low-amplitude earthquake. However, the residual displacement of the modelling result is not satisfying.

As it comes to complete damage level tests, the two modelling strategies show significant differences (see Fig. 8), especially in near-field (NF) cases. With considering sequential effects, the proposed model can produce better estimate of residual drift than that without considering sequential effects. Both methods can produce reasonable results in terms of peak drift, stiffness and cyclic degradation.

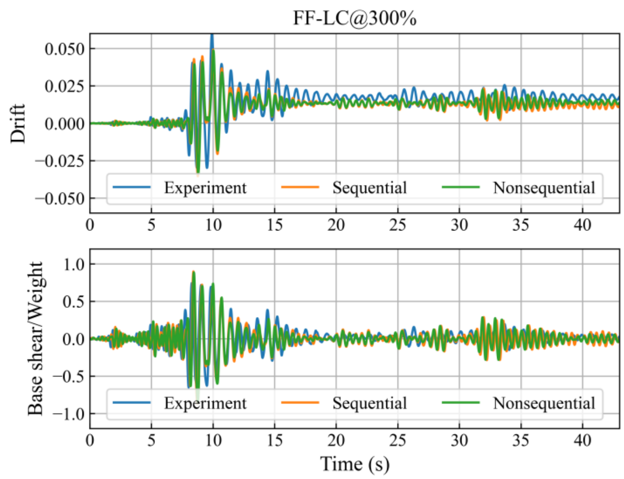

Fig.6. The experimental and numerical time-histories of normalised force and displacement (the FF-LC column in extensive damage level test)

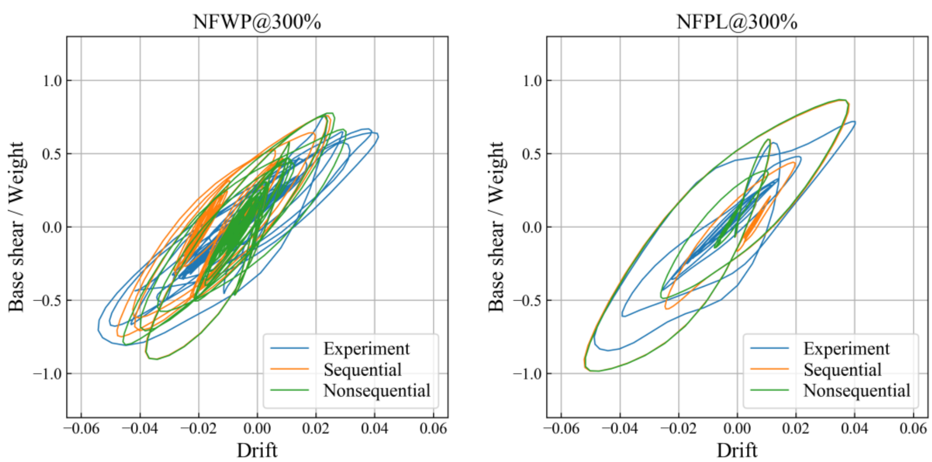

(a) (b)

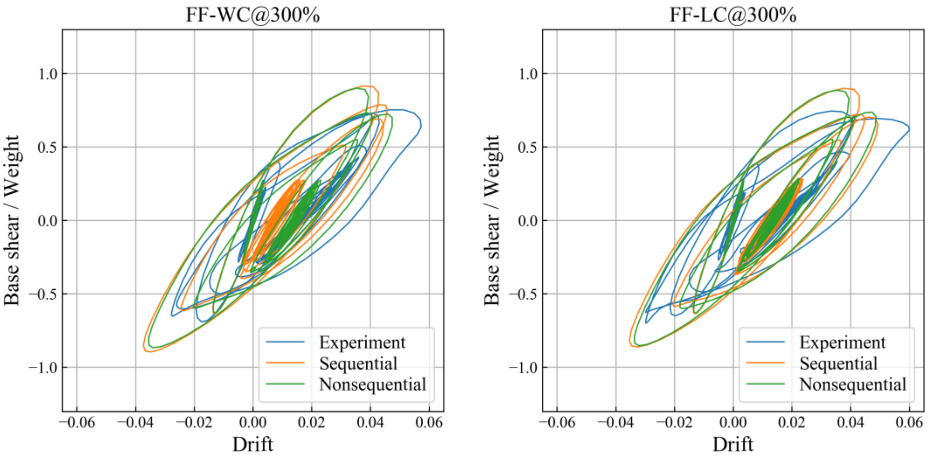

(c) (d)

Fig. 7. The modelling results in extensive damage level (300%) of all the specimens with/without consideration of the MSAS sequence.

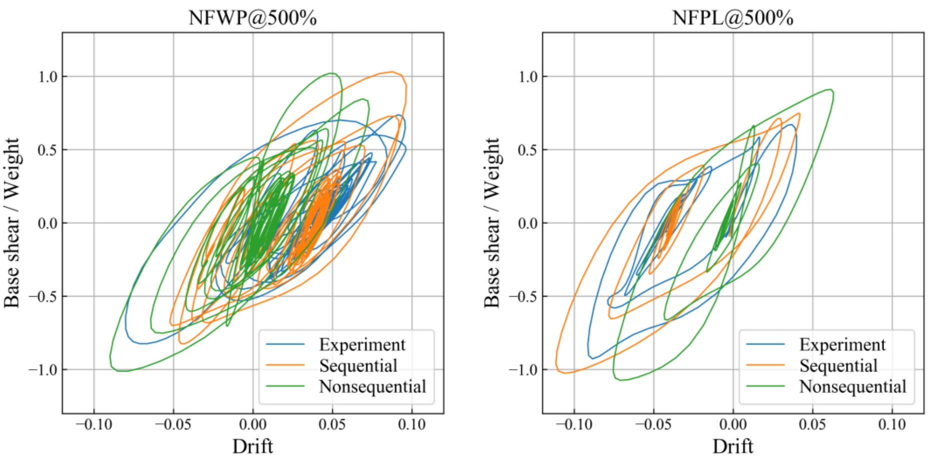

(a) (b)

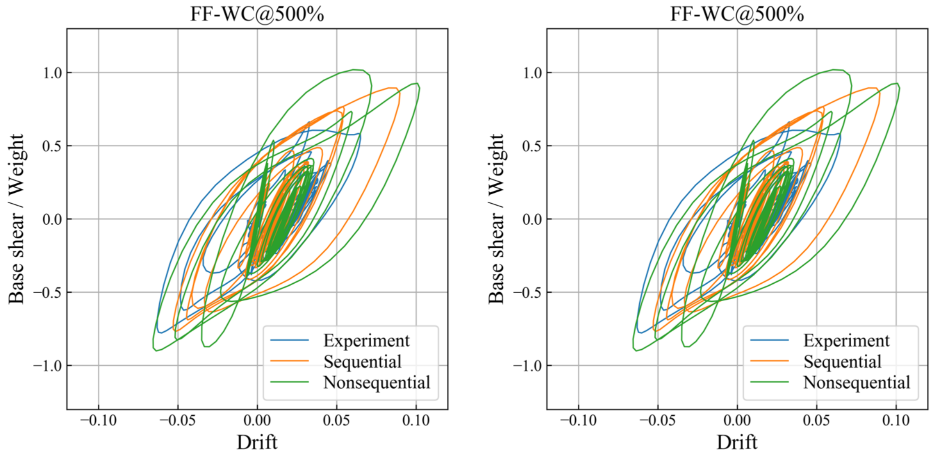

(c) (d)

Fig. 8. The modelling results in complete damage level (500%) of all the specimens with/without consideration of the MSAS sequence.

In aftershock tests, the proposed numerical model shows acceptable modelling results (see Fig. 9), especially in stiffness estimate. Compared to the extensive damage level modelling, although the ground motion intensity is exactly same, the accuracy of aftershock modelling results is not comparable to the previous ones. This is attributed to that the previous three-round tests have caused cumulative damage. In MSAS sequence, the cumulative error of the modelling of the RC column is generated during the MSAS sequence.

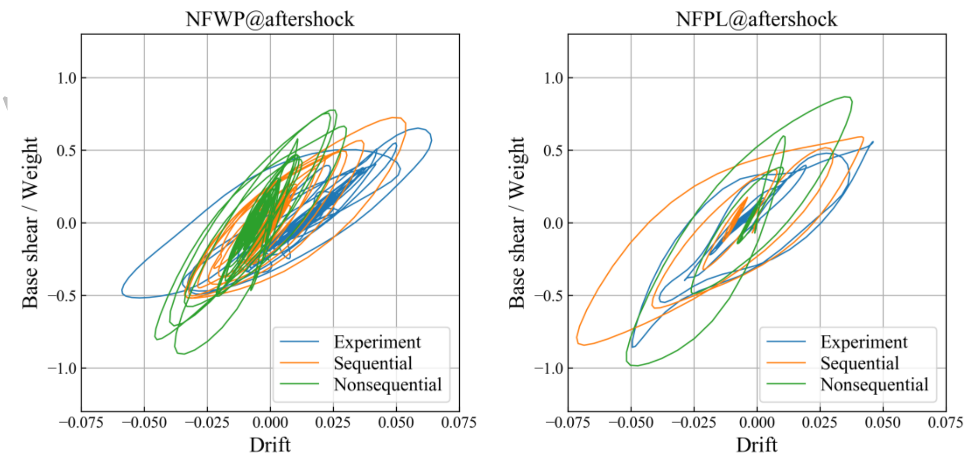

(a) (b)

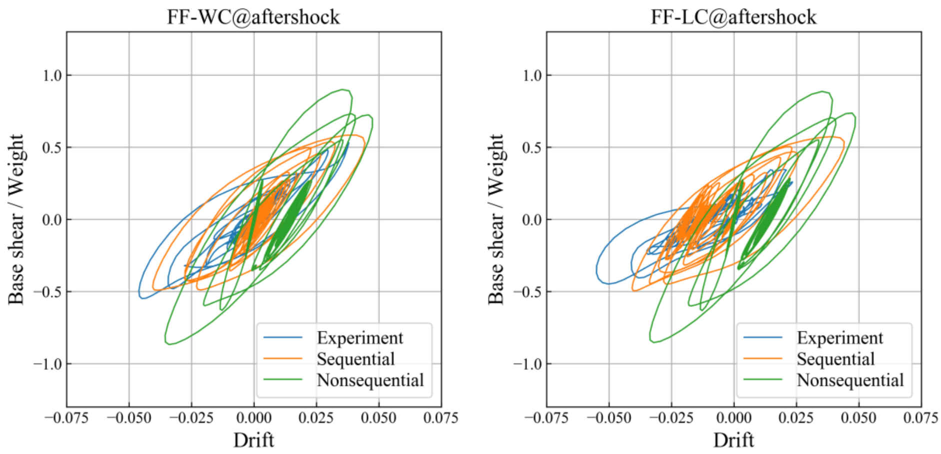

(c) (d)

Fig. 9. The modelling results in aftershock (300%) of all the specimens.

Based on the force-displacement loops, the hysteresis, peak deformation, permanent displacement can be obtained. To quantitatively evaluate the structural damage, the energy dissipation during the test is needed. In this work, the experimental specimen is simplified as a single degree of freedom (SDOF) system. The cumulative energy dissipation W can be obtained by Eqn. 7 [44].

$$W = -\int F(x, \dot{x}, t)dx \quad (7)$$

where F and x represents base shear and displacement response of the columns. It worth motioning that damping energy is neglected in the calculation process due to the difficulty of capturing the instantaneous damping force during the shaking table tests. To keep the consistency, the calculation of energy dissipation based on the modelling results follows the same manner. In slight damage level (25%) test, the dissipated energy plot of FF-WC is shown in Fig. 10 as an example. The numerical model considering concrete tensile behaviour has a good match against the experimental result. The numerical model neglecting concrete tensile behaviour overestimates the work done by the specimen during the test, which is in agreement with the larger force-displacement response shown in Fig 5. The energy dissipation plots of the four columns in extensive damage level (300%) tests are shown in Fig 11. The result shows that the proposed numerical model has good performance in modelling energy dissipation of RC column in seismic events. Considering cumulative damage in sequential input ground motion series can improve the accuracy of dissipated energy modelling, especially in the two FF specimens.

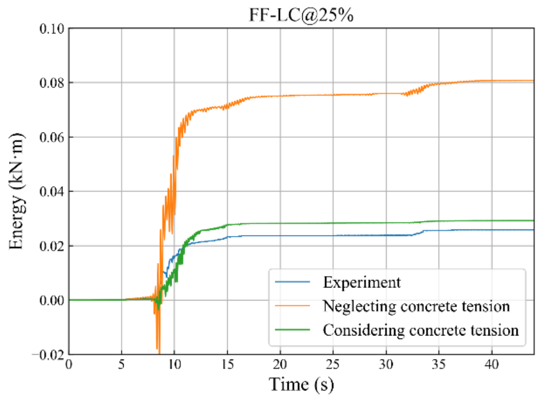

Fig. 10. Energy dissipation of FF-WC in slight damage level (25%) test and modelling results based on confinedconcrete01 and confinedconcrete01 with tensile branch.

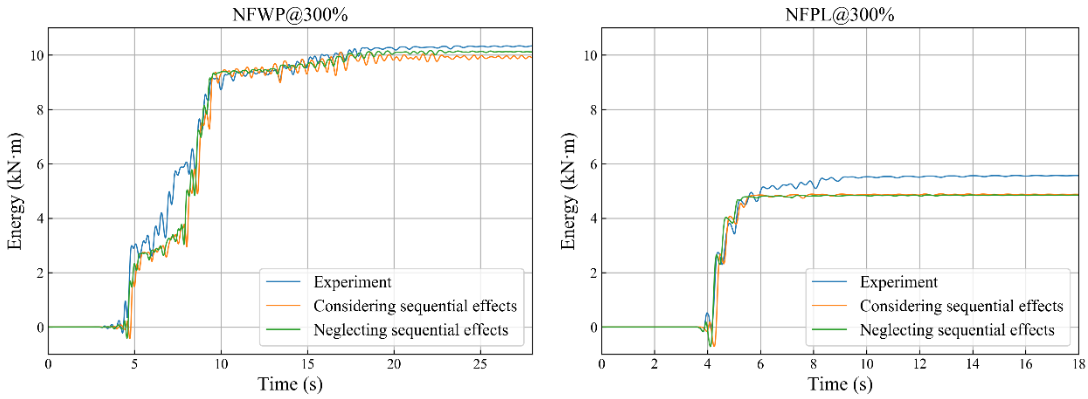

(a) (b)

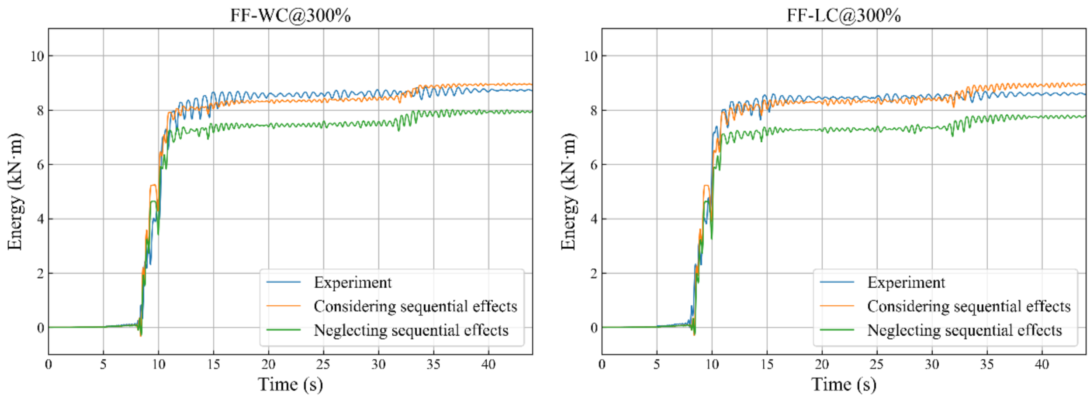

(c) (d)

Fig. 11. Energy dissipation of all the specimens in extensive damage level (300%) tests.

Correlation between ground motion intensity and bridge pier damage

In performance-based design, drift ratio is the most commonly used factor to predict the structural behaviour in seismic events. With the proposed numerical model above, the incremental dynamic analysis (IDA) can be performed to evaluate the seismic behaviour of the RC bridge pier excited by ground motions with increasing intensities. In the experimental work, due to the limit of shaking table load capacity, the axial load of the specimen is relatively small. In the numerical analysis work, the axial load is increased to 30 tonnes (about 16% axial load capacity).

The sequential earthquake effects are considered. In seismology, an aftershock is sparked by the mainshock. The PGA of an aftershock is not supposed to greater than that of the corresponding mainshock. In this work, different PGA ratios between aftershock and mainshock, γ, are considered (see Eqn. 8). Zhai et al. [7] suggest that if $\gamma < 0.5$, the effects of aftershocks are slight, which can be ignored. Therefore, the PGA ratios (γ) of 1.0, 0.8 and 0.5 are considered in this work. In earthquake events, aftershocks occur hours or even days later after the mainshock [45]. Therefore, a 4-second input ground motion with 0-amplitude is added between mainshock and aftershock records to make the column recover from vibrating.

$$\gamma = \frac{PGA_{AS}}{PGA_{MS}} \tag{8}$$

The IDA curves can indicate the relationship between seismic demand and capacity. The IDA requires two components: the intensity measure (IM) of the input ground motion and corresponding structural dynamic response. Peak ground motion acceleration (PGA) and spectral acceleration are commonly used as IM of a given ground motion record. The specimens (well-confined and low-confined) in this work have similar natural frequencies. Spectral accelerations of the ground motion for the types of the columns are close, which is proportional to the PGA. Therefore, PGA is selected as IM in this work.

The peak drift-PGA curves are plotted in Fig. 12. It is worth mentioning that residual displacement/drift is another important indicator of the inelastic response of the pier. It can be regarded as reference of damage and repair assessment. The residual drift-PGA curves of the two types of the columns under MSAS ground motion are plotted in Fig. 13. The dissipated energy-PGA curves are plotted in Fig. 14. As mentioned above, the damping energy is neglected in the experimental data processing due to the lack of reliable real-time damping force recording. However, the *OpenSees* model can produce time-histories of the damping force. Therefore, after taking damping into account, the dissipated energy calculation can be amended to the following:

$$W = -\int F(x, \dot{x}, t)dx + \int F_D(t)dx \tag{9}$$

where F_D refers to the damping force.

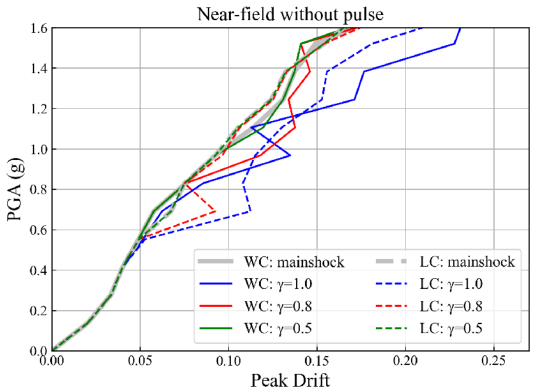

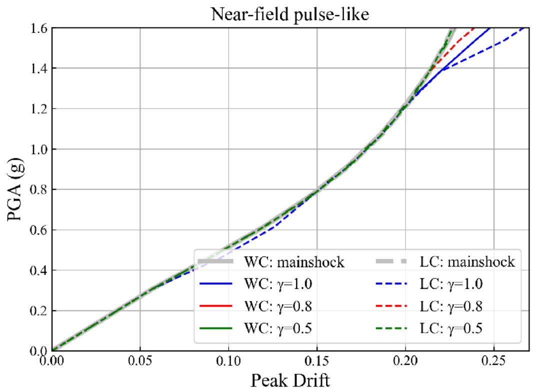

(a) (b)

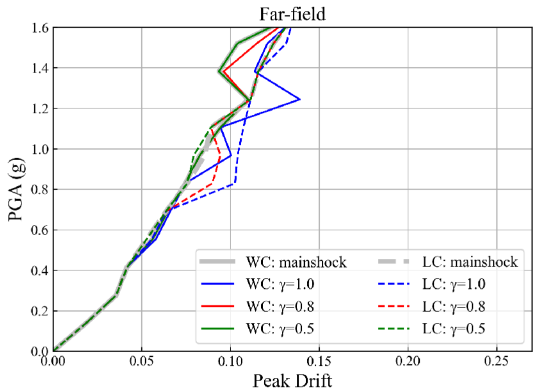

(c)

Fig. 12. The IDA curves (peak drift) of well-confined (WC) and low-confined (LC) columns in (a) NFWP, (b) NFPL and (c) FF ground motion cases.

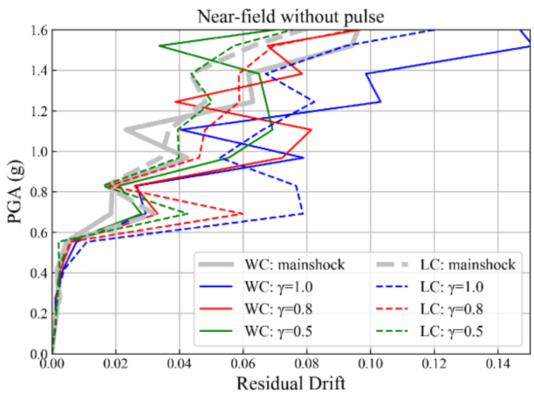

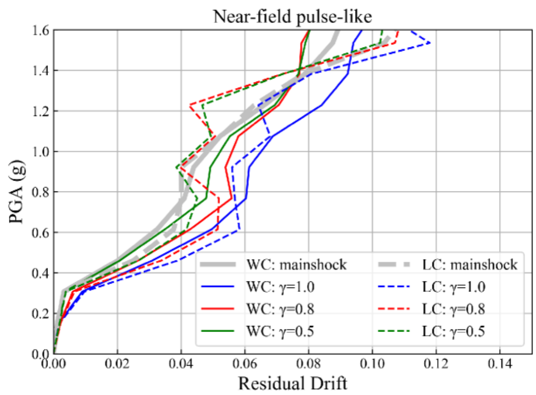

(a) (b)

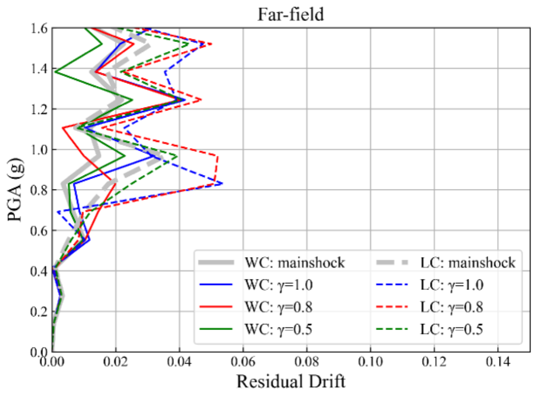

(c)

Fig. 13. The IDA curves (residual drift) of well-confined (WC) and low-confined (LC) columns in (a) NFWP, (b) NFPL and (c) FF ground motion cases.

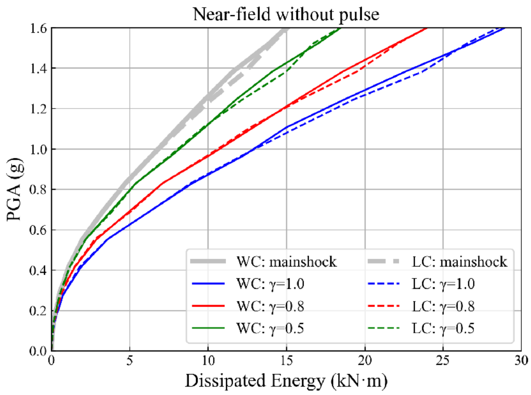

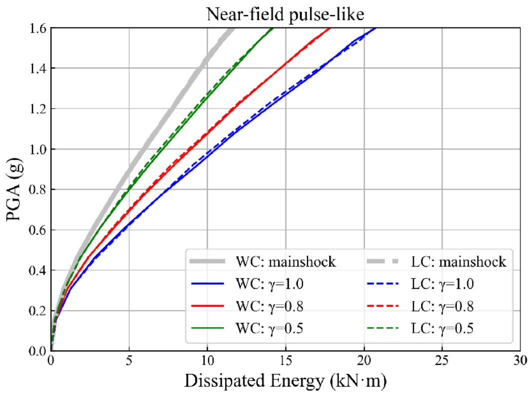

(a) (b)

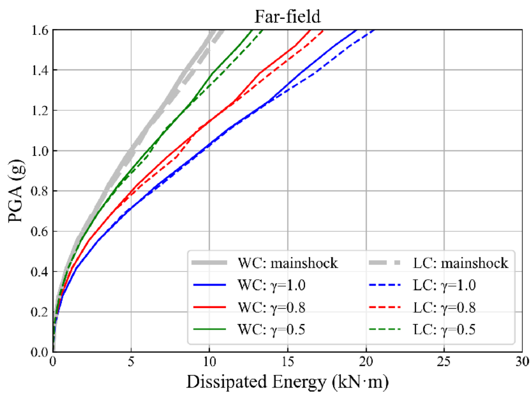

(c)

Fig. 14. The IDA curves (dissipated energy) of well-confined (WC) and low-confined (LC) columns in

(a) NFWP, (b) NFPL and (c) FF ground motion cases.

Fig. 12. illustrates that when the peak drift is less 5%, there is no significant difference between curves with/without considering MSAS effects in NFWP and FF cases. When the PGA of input ground motion is greater than 0.5g, the records with different PGA ratios result in different peak drift ratios. When $\gamma = 0.5, 0.8$, the peak drift ratio curve is close to the curve of mainshock in both well-confined and low-confined cases. When γ=1.0, the columns show larger drift in aftershocks than that in mainshocks. In NFPL case, the difference not observable until the drift reaches 20%. This is due the damage on the column is mainly caused by the velocity pulse contained in the ground motion. However, structures are not supposed to reach this level of large drift in seismic design. Seismic design code uses 5% drift as criteria to identify complete collapse of RC structures. Generally, the results show the curves are same when the drift of the column is within 5%, no matter they are excited by mainshock or aftershocks with different PGA ratios (γ). Therefore, using drift as EDP will underestimate the effects of aftershock damage in seismic design.

Fig. 13 shows the IDA curves of residual drift in mainshock only and MSAS cases. In the NFWP and NFPL cases, when $\gamma = 0.5, 0.8$, the mainshock and MSAS cases have similar residual drift. When $\gamma = 1.0$, the MSAS cases have significantly larger residual drift. When the drift of the column is smaller than 5%, larger residual drift can be found in lower-confined columns in both cases. Also, the NFPL cases generally have larger residual drift than the NFWP cases, which suggests the pulse contained in the near-fault ground motion causes severer permanent damage. The residual drift of the FF columns is significantly smaller than the NFWP and NFPL columns. In FF cases, lower-confined columns show larger residual displacement. The influence of PGA ratio (γ) on the FF columns is insignificant.

Fig. 14. shows using energy as EDP can get different IDA curves in mainshock only and MSAS cases. As expected, the columns have more energy dissipation with increasing γ. When $\gamma = 0.5$, the columns exhibits 20%-40% more energy dissipation in MSAS cases than mainshock only cases. When $\gamma = 0.8$, the columns exhibits 45%-55% more energy dissipation in MSAS cases than mainshock only cases. When $\gamma = 1.0$, the columns exhibits 75%-90% more energy dissipation in MSAS cases than mainshock only cases. The relation between PGA ratios and dissipated energy ratios between aftershock and mainshock is not straightforward. Therefore, the cumulative damage caused by aftershocks should be carefully considered. The low-confined column dissipates more than well-confined column due to its lower seismic capacity. In mainshock cases, columns excited by NFWP record show most energy dissipation compared with NFPL and FF cases, although NFWP record has shorter duration than FF record. The cumulative energy dissipation mainly governed by the effective duration rather than total duration. This is in agreement with authors' experimental findings [23].

Conclusion

In this paper, a numerical model is proposed and benchmarked against the shaking table tests on well-confined and low-confined specimens. The effect of concrete tension behaviour is examined. The behaviour of the proposed model in sequential earthquake events is investigated. With the calibrated model. A set of incremental dynamic analysis (IDA) is conducted on the two types of RC column. The difference in drift ratio and dissipated energy as engineering demand parameters (EDPs) is compared. Conclusions can be drawn as following:

1. The proposed numerical model exhibits the good performance of simulating the seismic behaviour of RC bridge pier excited different types of ground motion. The model can produce good results in terms of peak drift and dissipated energy. The residual drift

prediction is not always satisfying.

2. With/without considering aftershocks, the drift demand does not show significant differences when it is within the design range (e.g. 5%). Therefore, using peak drift alone as EDP could neglect the effects of aftershock. This is due that drift cannot precisely reflect the cumulative damage in MSAS cases.
3. With considering aftershocks, the RC bridge pier shows higher energy capacity demand in sequential earthquake events due to more cyclic energy dissipation. This should be taken into account when structural engineers design a bridge in a zone with potential mainshock-aftershock sequences.
4. The PGA ratio between aftershock and mainshock does not significantly affect the drift demand of RC bridge pier. However, it shows significances in energy capacity demand. With increasing PGA ratios, the higher energy capacity demand is found.
5. The non-stationary characteristics of MSAS series have significant influence on the peak drift, residual drift and energy dissipation of the bridge pier. This is in agreement with authors' previous experimental work [23].

Conclusion

This work has received financial support from the Natural Science Foundation of Hebei Province (project number: E2021202111) and the Open Research Fund Program of Guangdong Key Laboratory of Earthquake Engineering and Application Technology (project number: 2020B1212060071).

Reference

[1] Goda K. Nonlinear response potential of mainshock–aftershock sequences from Japanese earthquakes. Bull Seismol Soc Am 2012;102:2139–2156.

[2] Salami MR, Dizaj EA, Kashani MM. The behavior of rectangular and circular

reinforced concrete columns under biaxial multiple excitation. Comput Model Eng Sci 2019;120:677–91.
[3] Raghunandan M, Liel AB, Luco N. Aftershock collapse vulnerability assessment of reinforced concrete frame structures. Earthq Eng Struct Dyn 2015;44:419–39.
[4] Ryu H, Luco N, Uma SR, Liel AB. Developing fragilities for mainshock-damaged structures through incremental dynamic analysis. 9th Pacific Conf. Earthq. Eng., Auckland, New Zealand: 2011.
[5] Hosseinpour F, Abdelnaby AE. Effect of different aspects of multiple earthquakes on the nonlinear behavior of RC structures. Soil Dyn Earthq Eng 2017;92:706–25.
[6] Fayaz J, Xiang YJ, Zareian F. A Performance assessment of bridges under a sequence of seismic excitations. 7th Int. Conf. Comput. Methods Struct. Dyn. Earthq. Eng., Crete, Greece: 2019.
[7] Zhai CH, Wen WP, Li S, Chen ZQ, Chang ZW, Xie LL. The damage investigation of inelastic SDOF structure under the mainshock–aftershock sequence-type ground motions. Soil Dyn Earthq Eng 2014;59:30–41.
[8] Di Sarno L, Amiri S. Period elongation of deteriorating structures under mainshock-aftershock sequences. Eng Struct 2019;196.
[9] Amiri S, Bojórquez E. Residual displacement ratios of structures under mainshock-aftershock sequences. Soil Dyn Earthq Eng 2019;121:179–93.
[10] Kashani MM, Salami MR, Goda K, Alexander NA. Non-linear flexural behaviour of RC columns including bar buckling and fatigue degradation. Mag Concr Res 2018;70:231–47. doi:10.1680/jmacr.16.00495.
[11] Rodrigues H, Varum H, Arêde A, Costa A. Comparative effi ciency analysis of different nonlinear modelling strategies to simulate the biaxial response of RC columns. Earthq Eng Eng Vib 2012;11:553–66. doi:10.1007/s11803-012-0141-1.
[12] He ZY, Liu WA, Wang XW, Ye AJ. Optimal force-based beam-column element size for reinforced-concrete piles in bridges. J Bridg Eng 2016;21:06016006.
[13] Huang X, Kwon OS. Numerical models of RC elements and their impacts on seismic performance assessment. Earthq Eng Struct Dyn 2015;44:283–98.
[14] Laskar A, Mo YL, Hsu TTC. Simulation of post-tensioned bridge columns under reversed-cyclic loads. Mater Struct 2016;49:2237–56.
[15] Lin SS, Xia ZH, Xia J. Seismic damage model of bridge piers subjected to biaxial loading considering the impact of energy dissipation. Appl Sci 2019;9:1481.
[16] Ma HB, Zhuo WD, Lavorato D, Nuti C, Fiorentino G, Gu Y, et al. Probabilistic seismic response analysis on continuous bridges under near-fault ground motions. Iran J Sci Technol Trans Civ Eng 2019;43:491–500.
[17] Sun ZY, Wu G, Wu ZS, Zhang J. Nonlinear behavior and simulation of concrete columns reinforced by steel-FRP composite bars. J Bridg Eng 2014;19:220–34.
[18] Kashani MM, Lowes LN, Crewe AJ, Alexander NA. Phenomenological hysteretic model for corroded reinforcing bars including inelastic buckling and low-cycle fatigue degradation. Comput Struct 2015;156:58–71.
[19] Cassese P, De Risi MT, Verderame GM. A modelling approach for existing shear-critical RC bridge piers with hollow rectangular cross section under lateral loads. Bull Earthq Eng 2019;17:237–70.
[20] Terzic V, Schoettler MJ, Restrepo JI, Mahin SA. Concrete column blind prediction contest 2010: outcomes and observations. Berkeley, CA: 2015.

[21] McKenna F. OpenSees: a framework for earthquake engineering simulation. Comput Sci Eng 2011;13:58–66.
[22] Kashani MM, Lowes LN, Crewe AJ, Alexander NA. Nonlinear fibre element modelling of RC bridge piers considering inelastic buckling of reinforcement. Eng Struct 2016;116:163–77.
[23] Kashani MM, Ge X, Dietz MS, Crewe AJ, Alexander NA. Significance of non-stationary characteristics of ground-motion on structural damage: shaking table study. Bull Earthq Eng 2019:1–23.
[24] CEN.EN. Eurocode 2: design of concrete structures - Part 2: concrete bridges - design and detailing rules. Brussels, Belgium: 2005.
[25] CEN.EN. Eurocode 8 - Design provisions for earthquake resistance of structures - Part 2: Bridges. Brussels, Belgium: 2010.
[26] Correia AA, Almeida JP, Pinho R. Force-based versus displacement-based formulations in the cyclic nonlinear analysis of RC frames. 14th World Conf. Earthq. Eng., Beijing, China: 2008.
[27] Hall JF. Problems encountered from the use (or misuse) of Rayleigh damping. Earthq Eng Struct Dyn 2006;35:525–45.
[28] Charney FA. Unintended consequences of modeling damping in structures. J Struct Eng 2008;134:581–92.
[29] Jehel P, Léger P, Ibrahimbegovic A. Initial versus tangent stiffness-based Rayleigh damping in inelastic time history seismic analyses. Earthq Eng Struct Dyn 2014;43:467–84.
[30] Chopra AK, McKenna F. Modeling viscous damping in nonlinear response history analysis of buildings for earthquake excitation. Earthq Eng Struct Dyn 2016;45:193–211.
[31] Mohsenzadeh V, Wiebe L. Influence of damping model on computed collapse risk of special concentrically braced frames. 11th U.S. Natl. Conf. Earthq. Eng., Los Angeles, CA: 2018.
[32] Petrini L, Maggi C, Priestley MJN, Calvi GM. Experimental verification of viscous damping modeling for inelastic time history analyzes. J Earthq Eng 2008;12:125–45.
[33] Léger P, Dussault S. Seismic-energy dissipation in MDOF structures. J Struct Eng 1992;118:1251–69.
[34] Scott BD, Park R, Priestley MJN. Stress-strain behavior of concrete confined by overlapping hoops at low and high strain rates. ACI J Proc 1982;79:13–27.
[35] Braga F, Gigliotti R, Laterza M. Analytical stress–strain relationship for concrete confined by steel stirrups and/or FRP jackets. J Struct Eng 2006;132:1402–16.
[36] D'Amato M, Braga F, Gigliotti R, Kunnath S, Laterza M. A numerical general-purpose confinement model for non-linear analysis of R/C members. Comput Struct 2012;102:64–75.
[37] Filippou FC, Popov EP, Bertero V V. Effects of bond deterioration on hysteretic behavior of reinforced concrete joints. Berkeley, CA: 1983.
[38] Kolozvari K, Orakcal K, Wallace JW. Shear-flexure interaction modeling of reinforced concrete structural walls and columns under reversed cyclic loading. Berkeley, CA: 2015.
[39] Ballio G., Castiglioni CA. A unified approach for the design of steel structures under low and/or high cycle fatigue. J Constr Steel Res 1995;34:75–101.

[40] Uriz P. Towards earthquake resistant design of concentrically braced steel structures. University of California, Berkeley, 2005.
[41] Zhao J, Sritharan S. Modeling of Strain Penetration Effects in Fiber-Based Analysis of Reinforced Concrete Structures. ACI Struct J 2007;104:133–41.
[42] Ancheta T. D., Darragh RB, Stewart JP, Seyhan E, Silva WJ, Chiou BSJ, et al. PEER NGA-West2 Database. Berkeley, CA: 2013.
[43] Alexander NA, Chanerley AA, Crewe AJ, Bhattacharya S. Obtaining Spectrum Matching Time Series Using a Reweighted Volterra Series Algorithm (RVSA). Bull Seismol Soc Am 2014;104:1663–73. doi:10.1785/0120130198.
[44] Chopra AK. Dynamics of structures: theory and applications to earthquake engineering. 5th ed. Upper Saddle River, NJ: Pearson; 2016.
[45] Reasenberg PA, Jones LM. Earthquake hazard after a mainshock in California. Science (80-) 1989;243:1173–6.